J. COMBIN. MATH. COMBIN. COMPUT. 127a (2025) 449–468

Journal of Combinatorial Mathematics and
Combinatorial Computing
www.combinatorialpress.com/jcmcc

Combinatorial Press

Optimisation of digital preservation and 3D reconstruction of frescoes based on image processing algorithms

Xiaoqiang Tian[1], Xiaosheng Ding[1,✉]

[1] *Dunhuang Academy, Lanzhou, Gansu, 736200, China*

ABSTRACT

This paper is based on the digital image processing technology, using the undamaged image information to restore and protect the frescoes. The discrete binary wavelet change is used to decompose and denoise the image signal. And decompose and filter the high-frequency component and low-frequency component of the image, choose different components, respectively, carry out coefficient transformation, and solve the OMP least-paradigm for different random matrices. The color space is selected, and the mural color space is channel decomposed according to the grayscale mode and restored separately. Establish an assumed datum for each independent face of the mural, establish a spatial coordinate system for it, realize the transformation of spatial coordinates, and realize the super-resolution three-dimensional reconstruction of the mural based on the generative adversarial network and the self-attention mechanism. Objective evaluation indexes and subjective evaluation indexes are established to compare the protection effect of different algorithms on murals. Compared with the traditional algorithm CDD, this paper's algorithm improves the restoration time by 9.545~15.625 s, and the peak signal-to-noise ratio index improves by 1.35~4.769 db. In the results of the image extraction and processing, the calculated values of discrete curvature of the mural segments AB, CD, and EF ranges from -0.00945 to -0.00478, and the difference of standard deviation of the curvature from the target curvature is 6.477%. The approximate target curvature is obtained, and the algorithm has strong adaptive ability.

Keywords: digitized image processing, discrete binary wavelet variation, spatial coordinate transformation, self-attention mechanism, mural restoration

1. Introduction

Mural paintings are a combination of ancient art and culture, and are precious works of art, which not only record the living conditions of people in ancient times, but also reflect the ideology, culture, and religious beliefs of people in ancient times and other information. Due to the long history of mural paintings, the fragility of the materials used and the long time climate influence, water erosion, weathering, wind erosion,

✉ Corresponding author.
E-mail address: dhtt0937@163.com (X. Ding).

Received 08 June 2024; Revised 19 September 2024; Accepted 11 October 2024; Published Online 15 April 2025.
DOI: 10.61091/jcmcc127a-027

glacial erosion and other reasons, most of the mural paintings have been broken, peeling, fading, moisture, cracks and other problems [1-2]. Therefore, it is extremely important for the study of mural painting restoration technology.

The protection of frescoes is the biggest problem for cultural relics protection organizations, because frescoes are usually painted on the walls of buildings, tombs and grottoes, and the frescoes themselves are attached to the ground battle layer of the wall, and the destruction of the wall leads to the infringement of the frescoes as well [3-4]. At present, the repair of damaged frescoes mainly adopts the method of artificial repair, but the artificial repair has the problems of long cycle, high risk and irreversible results, which becomes a major obstacle to the repair of frescoes [5]. With the rapid development of photographic technology and the updating and iteration of equipment, many researchers have begun to apply cameras, scanners and other instruments to the digital conservation of murals [6-7]. Mural images are permanently preserved to pave the way for the next step of mural restoration, conservation and display. Through the digital image processing technology, the three-dimensional reconstruction and restoration of frescoes is a kind of modern technology for protection, restoration and cultural inheritance with high technology as the core, which provides a new idea for the digital preservation of frescoes [8-11]. This technology restores the color and texture of the original image as much as possible, which provides technical guidelines for the development of mural painting protection schemes to a certain extent, and makes the work difficulty of mural painting restoration drop steeply [12-14].

Cao, J. et al. proposed a consistency-enhanced generative adversarial network model as a mural restoration tool, under which a convolutional network extracts deep image features, optimizes the generative and discriminative network models for mural restoration through adversarial learning, and introduces a residual module to further optimize the network [15]. Yan, Y. et al. investigated the edge contouring repair method for broken mural paintings, and the proposed adversarial edge learning technique can not only quickly and accurately repair large areas of murals, but also repair the breaks and small missing parts of murals [16]. Li, J. et al. proposed a generator-discriminator network model for digital image restoration of broken murals based on artificial intelligence algorithms, which plays a great role in the repair of broken murals with point-like breaks and complex texture structures [17]. Xu, Z. et al. experimentally verified that the method combining the Unet network structure and the diffusion model has significant advantages in performing the fresco crack detection and digital restoration tasks, advancing the fresco crack restoration technology [18]. Kumar, K. M. P. et al. utilized a new straight line detection and extraction technique for convolutional computation of fresco images, and by weighting the original image with the averaged image under a filter averaging to realize virtual enhancement of mural images, which helps to restore the degraded patches of mural paintings [19]. Cao, J. introduced Adaptive Sample Block Local Search (ASB-LS) algorithm to improve Criminisi algorithm, which significantly improves the restoration of mural paintings in terms of subjective visualization, and at the same time improves the restoration efficiency of mural paintings [20].

Liu, Z. worked on deep learning techniques for mural image restoration, and believed that the design of deep learning network and the selection of loss function in the training process are important elements [21]. Xu, W. et al. examined the reliability of the DenseNet deep learning algorithm for mural color restoration and found that the algorithm produces better virtual restoration results compared to other other proposed model structures [22]. Gao, Z. et al. showed that since hyperspectral imaging technology can quickly and non-invasively obtain detailed spectral information on the surface of different categories of cultural artifacts, it has high scientific significance and application value for the conservation of ancient wall paintings [23]. Purkait, P. et al. explored high-quality synthesis and restoration methods for mural textures by applying block-based coherent texture synthesis techniques to interactive digital mural restoration [24].

This paper combines the use of photographic equipment and lighting equipment to realize high-definition digital image acquisition of murals, which lays the data foundation for the virtual restoration of murals. The discrete binary wavelet change is used to process the wavelet decomposition of the digitized image signals, and the matching tracking sparse reconstruction algorithm is used to solve the problem of the minimum number of paradigms of the model. Before performing the sparse transform, the improved wavelet change is used to separate the high-frequency component from the low-frequency component, and different components are selected to perform the sparse transform separately. The color space is selected for channel decomposition to ensure the restoration effect. An assumed datum is established for each wall surface of the mural caves, and control measurements and coordinate transformations are carried out sequentially for these caves to obtain the spatially varying coordinates of the image points, and to establish a three-dimensional reconstruction information model. Associative generative adversarial network and self-attention mechanism are used to complete the optimization of super-resolution 3D reconstruction of wall paintings. The objective and subjective image quality evaluation indexes are used to assess the conservation and reconstruction effect of the mural paintings.

2. Digital preservation techniques and applications for wall paintings

2.1. Digital protection

The significance of digitization of cultural heritage lies in the use of modern mapping, remote sensing and computer virtual reality technologies to record, preserve and protect cultural heritage, while promoting research, education and communication so that it can be more easily disseminated and shared, and the application of digitization technologies provides new possibilities for the use and transmission of cultural heritage.

Using digital means to record the whole picture of cultural heritage not only avoids the risk of data loss when cultural relics face various negative factors, but also provides the necessary technical support for follow-up research. At the same time, a database is established based on the collected information, and artificial intelligence technology is utilized to improve the processing efficiency and dissemination process of resource archives. For cultural relics that have been damaged or disappeared, re-presenting their appearance through digital means will help people better understand the real face of cultural heritage. In addition, for some cultural relics that require specific environments to show their real semantics, reconstructing their appearances and environments with the help of virtual reality technology will help people to recognize their connotations in depth. Digital display and dissemination breaks through the limitations of time and space, so that anyone can easily obtain the required information at any time and any place, and various exhibition methods also increase the audience's interest in viewing.

2.1.1. Image information acquisition. The use of photographic equipment combined with lighting equipment can realize the acquisition of high-definition digital images of murals. According to the different methods, shooting can be divided into visible light photography, microphotography and infrared photography. Visible light photography is used to obtain the overall picture of the fresco information. In the actual shooting, for small murals can be a one-time overall shooting. For large murals, in order to ensure image quality, to avoid the impact of lens aberrations, need to be shot in pieces, and then spliced in the computer to complete the acquisition of the whole mural. Micrographics can extract more detailed information about the mural, such as detailed texture, pigment granularity, painting marks and mold. Compared to visible light, near-infrared light penetrates certain pigments more easily, so lines that are more difficult to observe with the naked eye can be detected using a near-infrared camera.

2.1.2. Digital restoration of wall paintings. Digital information collection lays the data foundation for the virtual restoration of frescoes. Traditional fresco restoration methods require experienced experts to analyze, copy, and make up the color and other operations, which are time-consuming, costly, and affected by subjective factors. Digital image restoration processing refers to the use of computers to automatically repair mutilated images, aiming to make the image complete and in line with the human visual experience. The use of image restoration technology to restore broken murals can realize virtual restoration and virtual display, while providing a reference basis for subsequent artificial restoration. Digital restoration is retrospective and can avoid irreversible damage caused by manual restoration to a certain extent, which is crucial for the protection of mural paintings and cultural relics.

2.2. *Application of digital image technology in mural painting conservation*

2.2.1. Digital image processing techniques. Digital image restoration technology refers to the loss or damage of digital images, the use of undamaged image information, according to certain rules to fill in, so that the restored image is close to or to achieve the visual effect of the original image. The essence of image restoration technology is the learning of visual cognitive process, this paper analyzes from the perspective of visual psychology, based on the visual cognitive restoration law, and puts forward a variety of assumptions to qualify to solve the problem. In the restoration of murals, the peripheral information is fuzzy and untrustworthy, and the direct confrontation is that the front and back views are difficult to distinguish, and the breakage, blurring, noise, and color change exist at the same time.

2.2.2. Digital mural image denoising:

1) Realization of standard wavelet coefficient product. The standard equally spaced wavelet coefficient product is realized by wavelet decomposition of the signal using discrete binary wavelet transform. The discrete binary wavelet transform (DBWT) and discrete wavelet transform (DWT) algorithm structure is the same, the difference is that: DBWT is obtained by inserting $2^i - 1$ "0" between the neighboring coefficients of the DWT, and there is no down-sampling for each wavelet decomposition [25]. The advantages of DBWT are as follows. First, each wavelet decomposition of the signal produces equally spaced wavelet coefficients that are the same as those of the original signal, so that the product of equally spaced wavelet coefficients can be realized. Second, selecting the wavelet threshold becomes relatively easy. The reason is that in the DBWT domain, the signal redundancy is strong and the perturbation of some of the wavelet coefficients does not bring about serious distortion of the reconstructed signal. The definition of the product of two neighboring standard wavelet coefficients of the wavelet transform is given below:

$$PW_{j.k}^{i} = W_{j.k}^{i} * W_{j+1.k}^{i} \quad i = 1 \text{ or } i = 1, 2, 3,\ j = 0, 1, \ldots, j\text{-}1 \tag{1}$$

where "*" denotes the dot product operation of two vectors or matrices, and W_{jk}^{i} and W_{j+1k}^{i} are the wavelet coefficient vectors (one-dimensional) or matrices (two-dimensional) of the j rd and $j+1$ th distances, respectively.

2) Compression perception. In general, a signal X of length N in R^N can be represented as:

$$x = \sum_{i=1}^{x} \psi_i \theta_i\,, \quad X = \psi\theta \tag{2}$$

where: ψ is the standard orthogonal basis of $N \times N$, θ is the coefficient vector of the signal X expanded in this orthogonal basis, ψ_i is the column vector in the orthogonal basis ψ and θ_i is the element in the $N \times 1$ dimensional coefficient vector θ. A signal X is said to be K sparse in the orthogonal basis ψ if only K elements of the coefficient vector θ are not zero and $K \ll N$.

After obtaining the sparse coefficient vector $\theta = \psi^{\mathrm{T}} x$ of the signal by transformation, an observation matrix $\Phi(M \times N)$ is then used to obtain the $M(M < N)$ observations. The process is denoted as:

$$Y = \psi\theta = \Phi\Psi^T X = A^{cs} X \tag{3}$$

where Y is the observation vector and A^{cs} is called the compressed perception matrix. If Y and Φ are known, it is required to solve θ because $M < N$, the system of equations (3) has no solution and is an underdetermined system of equations. If θ is sparse and A^{cs} has the finite isometric property (RIP), the system of equations can be solved for a unique sparse solution. The solution method is:

$$\left.\begin{array}{r}\arg\min \|\theta\|_1 \\ s.t. Y = \Phi\theta\end{array}\right\} \tag{4}$$

For Eq. (4) can be solved using gradient projection method, basis tracking method, matching tracking method, orthogonal matching tracking method, etc., and then reconstruct the recovered signal. In mathematical sense, the signal reconstruction problem based on compressed perception theory is to find the underdetermined system of equations.

3) Minimum L_0-parameter model. The L_0-parameter model portrays the number of nonzero elements in the signal, thus making the result as sparse as possible. The minimum L_0-parameter optimization problem is usually described by the following equation:

$$\left.\begin{array}{r}\min \| X \|_0 \\ s.t. Y = \Phi X\end{array}\right\} \tag{5}$$

In practice, some degree of error is allowed to exist, so the original optimization problem is transformed into a simpler approximate form of solution where δ is a very small constant:

$$\left.\begin{array}{r}\min \| X \|_0 \\ s.t. \| Y - \Phi X \|_2^2 \leq \delta\end{array}\right\} \tag{6}$$

However, the numerical computation for solving such problems is extremely unstable and difficult to solve directly.

The common algorithms demonstrated in current research include three categories: 1) greedy tracking methods, such as the OMP algorithm and the MP algorithm, 2) convex relaxation methods, such as the interior point method, and iterative thresholding, and 3) combinatorial algorithms, such as Fourier sampling, and HHS tracking.

The match-tracking class of sparse reconstruction algorithms solves the minimum L_0-parameter problem, and the earliest proposed are the match-tracking (MP) algorithm and the orthogonal match-tracking (OMP) algorithm [26].

2.2.3. Matching tracking algorithm. The OMP uses a compressed projection of the K-sparse signal x to measure the signal Φ, OMP in a K iteration process to select the element with the highest correlation with the residuals into the estimation of the support set, and then a least squares orthogonal projection process is used to update the estimated signal. The basic idea of the matching tracking algorithm is to select the atom that most closely matches the signal from a library of overcomplete atoms (i.e., the perceptual matrix) during each iteration to perform the sparse approximation and derive the residual, and then continue to select the atom that most closely matches the signal residual. After several iterations, the signal can then be represented linearly by a number of atoms. However, due to the non-orthogonality of the projection of the signal on the set of selected atoms (column vectors of the perceptual matrix), the result of each iteration may be sub-optimal, and thus a higher number of iterations is often required to obtain better convergence results.

The match-tracking class algorithm calculates the correlation coefficient by finding the absolute value of the inner product between the residual r and the individual atoms in the perceptual matrix Φ:

$$R = \{ R_j \mid R_j = |\langle r, \varphi_j \rangle|, j = 1, 2, \cdots, N \} \tag{7}$$

And the least squares method is used for signal approximation as well as margin updating [27]:

$$\hat{X} = \underset{i \in R^A}{\arg\min} \| Y - \Phi_\Lambda X \|_2 \tag{8}$$

2.2.4. Improved OPM algorithm. Before doing the sparse transform, the improved wavelet transform is used to decompose and filter the high-frequency and low-frequency components, and different components are selected for the sparse transform, and the sparse matrix will be transformed by the wavelet and different random matrices will be selected for the solution of the minimum number of paradigms of the OMP matrix equation when reconstructing the image, and the steps of the improved OMP algorithm are as follows:

1) Select the wavelet function suitable for mural features to construct the high-frequency components and low-frequency components.

2) Turn to sparse matrix and construct orthogonal matrix [28].

3) Calculate the mural features. The correlation coefficient of color and contour $\{\langle R_k f, x_n\rangle; x_n \in D,\ D_k\}$ is found $x_n+1 \in D,\ D_k$, as in $|\langle R_k f, x_{n+1}\rangle| \geq a \sup |R_k f, x_j| \, 0 < \alpha \leq 1$.

4) Stop when $|\langle R_k f, x_{n+1}\rangle| < \delta, (\delta > 0)$. Record D from $1, 2, \cdots, k+1$.

5) Calculate:

$$x_{n+1} = \sum_{n=1}^{k} b_n^k x_n - \gamma_k \quad \langle x_n, \gamma_k \rangle 0, n = 1, 2, \cdots, k \tag{9}$$

Setting:

$$a_{k-1}^{k+1} = \alpha_k = \|r_k\|^{-2} \langle R_k f, x_{n+1}\rangle \, a_n^{k-1} = a_n^k - a_k b_n^k \tag{10}$$

Update the following quantities:

$$f_{k+1} = \sum_{n}^{k+1} a_n^{k+1} x_n, \quad R_{k+1} f = f - f_{n+1} \tag{11}$$

$$D_{k+1} = D_x \cup \{x_{n+1}\} \quad |\langle R_n f, x_{n+1}\rangle| \langle \delta, (\delta\rangle 0), k \leftarrow k+1 \tag{12}$$

6) Otherwise stop the iteration, then repeat steps (3) to (7). Finally output the approximation of x.

2.3. *Gray scale decomposition of mural images*

Murals are generally color, color images and grayscale images is different in that color images are composed of red, green and blue (RGB) three-band data that have a certain correlation with each other. Since the three channels R, G and B of the RGB space have correlation, the restoration is not effective. Therefore, in order to achieve better restoration results, $L\alpha\beta$ color space is selected for channel decomposition, and then restored separately.

$L\alpha\beta$ Color space is based on data-driven research on human perception, which assumes that the human visual system is ideally adapted to the processing of natural scenery, where L is a non-color component denoting luminance values, α denoting yellow- and blue-related color values, and β denoting red-a-green-related color values. The $L\alpha\beta$ -color space basically eliminates the correlation between the components and is the most compatible with human visual perception, therefore, the $L\alpha\beta$ -color space is chosen to be used for channel decomposition to achieve the restoration of color images. For the broken murals, the images are first converted from RGB color space to LMS space, and then LMS space is converted to $L\alpha\beta$ color space. Using the transformation algorithm of $L\alpha\beta$ color space, the image of the mural was decomposed into three grayscale images L, α, β according to the three channels of $L\alpha\beta$ color space.

2.4. *Wall painting image edge detection*

Cracks and localized pigment shedding are common defects in ancient paintings such as ancient murals. Cracks are mainly caused by aging, drying, thermal expansion and contraction due to temperature change, or mechanical failure, etc., while shedding is mainly caused by natural factors such as diseases, earthquakes, or man-made damages, which result in localized pigment peeling off from frescoes and other ancient paintings, or localized stains that cannot be removed and covered by them. Detecting and dividing these defective areas is a prerequisite for the diagnosis and virtual restoration of ancient paintings such as frescoes, and a lot of related research has been done. Detection steps:

1) Filtering. Edge detection is mainly based on derivative calculation, but is affected by noise. The filter reduces the noise and also leads to the loss of edge strength.

2) Enhancement. The enhancement algorithm highlights the points in the field that have significant changes in gray scale. This is generally done by calculating the gradient magnitude.

3) Detection. However, in some images with large gradient magnitude are not edge points.

4) Localization. Determine the location of the edge precisely.

2.4.1. Crack Detection and Segmentation of Mural Images. Crack detection includes both semi-automatic and fully automatic methods. Since the cracks of artwork have the characteristics of being darker than the background and having a more consistent gray scale, the semi-automatic method mainly locates the cracked area by utilizing these two characteristics, by selecting the seed point by the user, and then growing and tracking the area, whereas the fully automatic method also defines a certain suitable filter to filter the image based on the above two characteristics, and then sets the suitable threshold to filter out the cracked area, and this method Often, strokes with similar characteristics are also detected at the same time, so it is necessary to use classification algorithms to eliminate non-cracked object areas based on the above results according to the color and other characteristics. For the segmented cracks, some kind of interpolation algorithm is generally used for automatic repair.

2.4.2. Image Shedding Region Detection and Segmentation. For the detection and segmentation of shedding region, the current methods can be mainly categorized into semi-automatic and fully automatic. et al. proposed a semi-automatic method that can better segment the shedding blank part of ancient oil paintings to segment the shedding region by using the improved region growth algorithm, which increases the consideration of color information when segmenting out the shedding region, so that it is more in line with the habit of artificial recognition and can obtain better results. Due to the complex structure of murals and rich texture information, it is difficult to detect the broken region for some images with edge detection technology, and in this paper, we use the method of artificial calibration to determine the broken region.

3. Optimization of three-dimensional reconstruction of wall paintings

3.1. Control measurements and coordinate transformations

In order to generate a digital surface model (DSM) for each wall mural, an assumed datum plane is established for each wall mural in the cave, and the original measured coordinates of the control points of that wall are converted into spatially assisted coordinates based on that assumed datum plane [29]. The coordinate origin of each wall is located in the lower left corner of the assumed datum plane, and the datum plane is used as the bottom plane to establish three-dimensional spatial auxiliary coordinates so that the Z-axis is perpendicular to the datum plane. In order to make the result of coordinate conversion clear at a glance, when establishing the assumed datum plane, try to ensure that the Z value after the original control point coordinate conversion is positive. Since the origin of each coordinate system is chosen at the turning point of the cave outline, in order to ensure that the Z-value is positive, we have re-established a wide outline frame for the cave according to the coordinates of the control points in the original coordinate system and in accordance with the shape of the cave, so as to ensure that the coordinates of the original control points, after being rotated, can all fall on the datum plane with the turning point of the new outline of the cave as the origin.

The spatial coordinate transformation of an image point is the transformation of the image point's image-space Cartesian coordinates $(x, y, -f)$ to image-space auxiliary coordinates (X, Y, Z). This is the problem of transforming the coordinates of the same image point in two spatial Cartesian coordinate systems with the same origin. The expression is shown in (13):

$$\begin{bmatrix} x \\ y \\ z \end{bmatrix} = R \begin{bmatrix} x \\ y \\ -f \end{bmatrix} \tag{13}$$

Among them:

$$R = \begin{bmatrix} a_1\, a_2\, a_3 \\ b_1\, b_2\, b_3 \\ c_1\, c_2\, c_3 \end{bmatrix} = \begin{bmatrix} \cos Xx \cos Xy \cos Xz \\ \cos Yx \cos Yy \cos Yz \\ \cos Zx \cos Zy \cos Zz \end{bmatrix} \tag{14}$$

is the rotation matrix for the rotational transformation of the spatial axis system.

Matrix element $a_i, b_i, c_i (i = 1, 2, 3)$ is called the directional cosine a_1, a_2, a_3 is the cosine of the angle between axis X and axis x, y, z, b_1, b_2, b_3 is the cosine of the angle between axis Y and axis x, y, z, and c_1, c_2, c_3 is the cosine of the angle between axis Z and axis x, y, z.

3.2. *Recovery of three-dimensional information from digital images of wall paintings*

3.2.1. Establishment of survey areas and models. Figure 1 shows the mural digital image three-dimensional information recovery flow chart, first establish a measurement area, and input the measurement area parameters. Control points need to be converted from the original data in meters to centimeters. Photographic scale is 1/25, the number of air strips is 1, the image type is close-up photography, the DSM grid interval is 5cm, the contour line spacing is 5cm, the mapping scale is 1/1000, the resolution of the orthophoto is 400DPI, the resolution of the image element is 0.063mm, and the main image is selected as the left image. In the process of orthophoto correction, only the control point parameters are the only parameters that need to be known, and the other parameters can be set artificially according to the actual situation and specific requirements.

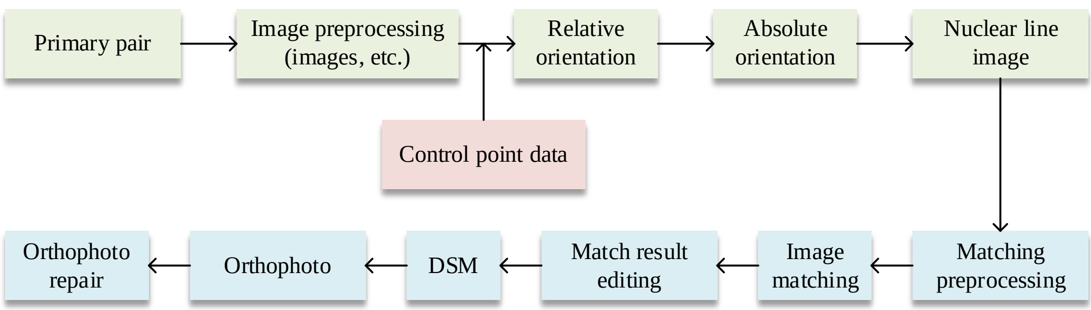

Fig. 1. Flow chart of 3D information restoration of Dunhuang murals digital images

3.2.2. Model orientation. Since the mural is treated as a non-metric camera, it does not need to be oriented internally, but only relatively oriented and absolutely oriented. The operation process of relative orientation is to find the control points with the same name in the control point file on the left and right image pairs in the module of relative orientation, and locate them precisely so as to minimize the residual difference of each control point, and also minimize the RMS value. The relative orientation is completed after at least 6 control points are precisely located. In the relative orientation process of the east wall, the number of automatically matched points is 246, the RMS is 5.5 mm, and the residuals of the control points are between ±0.010. Most of the residuals of the absolute orientation of the control points of the east wall are relatively small, at the level of 1/10 of a millimeter.

3.2.3. Nuclear line resampling. After solving the relative orientation parameters, the so-called kernel line queuing can be carried out on the original digital image, i.e., the original image is resampled according to the kernel correlation principle, and the upper and lower parallaxes in the Y directions are eliminated to form the kernel image pairs, which is a preparation for the automatic matching. Since the kernel image has eliminated the up and down parallax, the two-dimensional image matching process of searching for homonymous images is transformed into a one-dimensional searching process in the direction of the kernel, which greatly improves the efficiency and reliability of image matching.

3.2.4. Image Matching. In the image matching before doing some matching preprocessing work, mainly for some matching is more difficult to deal with some of the areas. For example, the four corners of the image is covered by the black shadow of the parts, the top of the Buddha's niche in the shape of the steep change in the parts, these places may not match the results, in the image before the matching preprocessing in order to obtain better matching results, thus reducing the matching of the editing of a large number of jobs.

3.3. *Super-resolution 3D reconstruction of wall paintings*

3.3.1. Generating Adversarial Networks. Generative Adversarial Networks (GANs), consisting of a generative network and a discriminative network, have been a popular model for deep learning in recent years. This network can be used to learn more difficult feature representations by randomly generating a large number of samples of different types. The generative adversarial network loss math equation is shown in equation (15):

$$\min_G \max_D V(D,G) = E_{x\sim P_x}[\log D(x)] + E_{z\sim P_z(z)}[\log(1-D(G(z)))] \tag{15}$$

where in x denotes a real high-resolution image, z denotes a real low-resolution image, p_x denotes a data distribution of a real high-resolution mural image, P_z denotes a data distribution of a reconstructed image, $E_{x\sim P_x}$ denotes a mathematical expectation of a probability distribution of a real high-resolution image, $E_{z\sim P_z(z)}$ denotes a mathematical expectation of a probability distribution of a reconstructed image, $D(x)$ denotes a probability of the discriminative network to judge whether or not the real image data is true or untrue, $G(z)$ denotes reconstructed image data, $D(G(z))$ denotes the probability that the discriminative network judges whether the reconstructed image is true or not, $\log D(x)$ denotes the result of the discriminative network's judgment of the true image, and $\log(1-D(G(z)))$ denotes the result of the discriminative network's judgment of the reconstructed image.

3.3.2. Self-attention mechanisms. Humans devote more attention to the focus area in the target image and ignore the detail information in the non-focus area, the advantage of doing so is that the limited visual attention resources can be utilized to quickly obtain the valuable information in the image, which is the human visual attention mechanism. The attention mechanism in neural networks is a mechanism that imitates the visual attention mechanism of the human brain In the process of neural network deep learning, the larger the amount of data received and processed by the model, the more valuable information the model acquires from the training set. In this paper, the attention mechanism is utilized in fully mining the context-associated features in the LR image in order to strengthen the importance of high-frequency features in the image, which helps to maintain the true and clear high-frequency texture detail information in the reconstructed mural, and to improve the visual effect of the image.

The formula of Scaled Dot-Product Attention mechanism (Scaled Dot-Product Attention) is shown in equation (16):

$$Attention(Q,K,V) = soft\max(QK^T / \sqrt{d_k})V \tag{16}$$

where, the dimensions of Q & K are the dimensions of d_k, v are The dimensions of d_v, Q, K, v are short for Query, Key, and Value, respectively. When d_k is too large, the variance of the inner product result of Q vs. K is large, and the inner product result is scaled in order to avoid the problem that the internal covariate shift leads to a smaller gradient of the SoftMax function. The dot product attention mechanism can be performed with the help of matrix operations to compute the Attention output vectors of all positions at once, thus improving the parallel computing capability.

3.4. Super-resolution reconstruction of frescoes based on self-attentive generative adversarial networks

3.4.1. Network structure. Figure 2 shows the structure of the generative network. After the low-resolution mural image (LR) is input to the generative network, the shallow features are first extracted by 1 convolution, and then the deeper features of the mural are extracted by the residual layer, which effectively solves the problem of gradient disappearance or gradient explosion brought by the network being too deep, and finally outputs the super-resolution mural image (SR) after the image is reconstructed by the reconstruction layer. Among them, the residual layer consists of 16 residual blocks, 1 convolution and jump-level connection, each residual block contains 2 convolutions and 1 PReLU activation function, and the reconstruction layer consists of 2 upsampling blocks, 1 convolution and 1 self-attention module, and the upsampling block contains 1 convolution and 1 sub-pixel convolution.

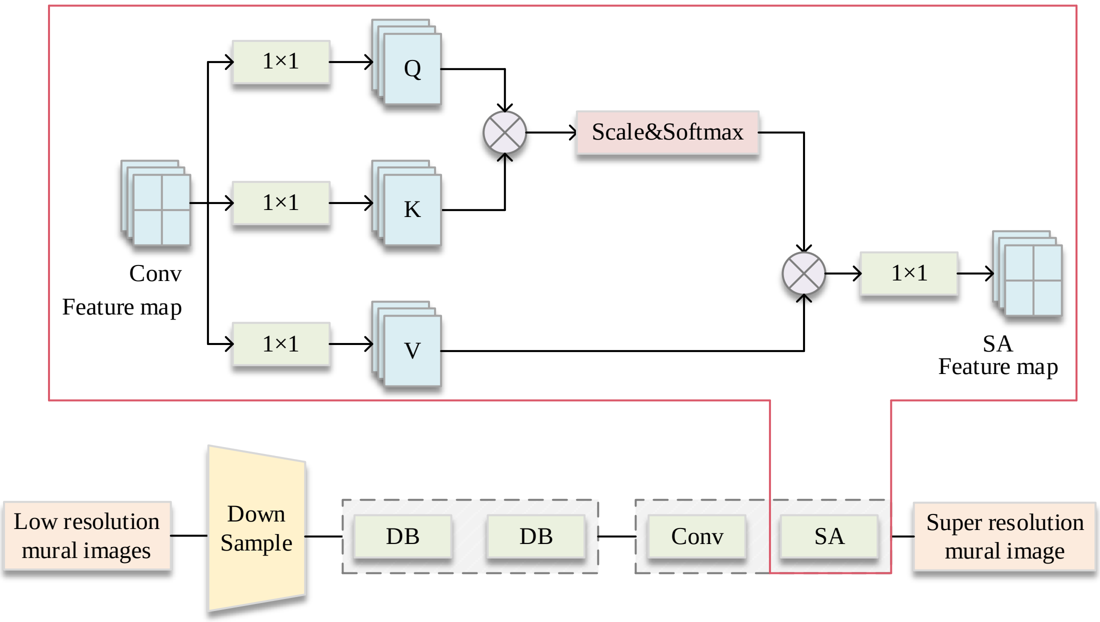

Fig. 2. Generating network structure

3.4.2. Activation functions. Although the ReLU activation function is fast to train, converges well and can avoid the problem of gradient vanishing, it is easy to cause the neural network to fall into a sparse state, i.e., it no longer participates in the updating of the network parameters, when the output of a certain neuron is zero. To solve this problem, this paper uses PReLU activation function in the generative network and LeakyRelu activation function in the discriminative network.PReLU activation function and LeakyRelu activation function are both variants of ReLU activation function, which guarantees that the activation function will have a non-zero output even if the input is less than zero.The difference between PReLU activation function and LeakyRelu activation function lies in the fact that PReLU activation function and LeakyRelu activation function can be used in the same way. The difference between the PReLU activation function and LeakyRelu activation function is that the hyperparameter α in the PReLU activation function is learnable and the hyperparameter α in the LeakyRelu activation function is a very small fixed value.The formula for the LeakyRelu activation function is shown in Eq. (17):

$$LeakyRelu(x) = \max(\alpha x, x) \tag{17}$$

3.4.3. Loss function. The role of the loss function is to estimate the difference between the output result of the network and the real data, i.e. the difference between the reconstructed fresco image (SR) and the real high-resolution fresco (HR), so that the network and the real data to establish a certain relationship between the network and the real data, and a good loss function can speed up the training speed of the network and improve the quality of the network, and the smaller the loss function is, the better the model is. In order to reproduce the realistic visual effect of the mural image, this paper uses the content loss and the antagonistic loss together to form the total loss function of the generative network. The total loss function formula is shown in equation (18):

$$l_G = l_{content}^{SR} + 10^{-3} l_{Gen}^{SR} \tag{18}$$

The content loss consists of pixel-by-pixel MSE loss and VGG loss, and the content loss function is calculated as shown in equation (19):

$$l_{content}^{SR} = l_{MSE}^{SR} + 10^{-3} l_{VGG}^{SR} \tag{19}$$

The MSE loss estimates the error between the reconstructed image and the real image pixel by pixel, and the MSE loss function is calculated as shown in equation (20):

$$l_{MSE}^{SR} = \frac{1}{r^2 WH} \sum_{x=1}^{rW} \sum_{y=1}^{rH} \left(I_{x,y}^{HR} - \mathrm{G}_{\theta_G} \left(I^{LR} \right)_{x,y} \right)^2 \tag{20}$$

where W and H denote the width and height of the image, respectively, r denotes the scaling factor, and $G_{\theta_G}(I^{LR})_{x,y}$ denotes the reconstructed image.

To compensate for the problem of missing high frequency details in the images generated by the model driven by the MSE loss, in this paper, the reconstructed image (SR) and the real high resolution image (HR) are fed into the pre-trained VGG19 network to obtain the corresponding feature maps, and the mean-square error between the VGG feature maps is computed to obtain the VGG loss. The computational formula for the VGG loss is shown in Equation (21):

$$l_{VGG}^{SR} = \frac{1}{WH} \sum_{x=1}^{W} \sum_{y=1}^{H} \frac{(\phi_{\mathrm{i,j}}(I^{\mathrm{HR}})_{x,y}}{\phi_{\mathrm{i,j}}(\mathrm{G}_{\theta_{\mathrm{G}}}(I^{\mathrm{LR}}))_{x,y})^2} \tag{21}$$

where W and H denote the width and height of the VGG feature map, respectively. ϕ_{ij} denotes the VGG feature map obtained through the j th convolutional layer before the i th maximum pooling layer.

The adversarial loss estimates the sum of the discriminative probabilities of all the training samples, making the data distribution of the reconstructed image closer and closer to the real image. The formula for the adversarial loss is shown in equation (22):

$$l_{Gen}^{SR} = \sum_{n=1}^{N} -\log \mathrm{D}_{\theta_{\mathrm{D}}}(G_{\theta_G}(I^{LR})) \tag{22}$$

where $\mathrm{D}_{\theta \mathrm{b}}(G_{\theta_G}(I^{LR}))$ denotes the probability that the discriminative network will judge the reconstructed image (SR) as the real image (HR).

3.4.4. Image quality evaluation indicators:

1) Peak signal-to-noise ratio (PSNR). PSNR is currently the most widely used, the longest history of a class of image quality evaluation index, defined as shown in equation (23):

$$PSNR = 10 \log_{10} \left(\frac{peak^2}{MSE} \right) \tag{23}$$

where peak represents the maximum possible value that can be achieved for a pixel and MSE is the mean square error, which measures the pixel differences between images. The definition is shown in (24):

$$MSE = \frac{1}{xy}\sum_{i=0}^{x-1}\sum_{j=0}^{y-1}\left[T(i,j) - R(i,j)\right]^2 \tag{24}$$

where, T is the original HD image, R is the super-resolution image obtained by reconstruction, x is the length of the image and y is the width of the image. From the above two equations, it can be known that the value of PSNR is directly proportional to the image quality, and at the same time, its value is closely related to the MSE, which belongs to the evaluation standard that focuses more on the difference of pixel gray value. This index does not take into account the visual characteristics of the human eye (the human eye is more sensitive to contrast differences with lower spatial frequency, the human eye is more sensitive to luminance contrast differences than chromaticity, and the results of the human eye's perception of an area will be affected by its surrounding neighboring areas, etc.), and thus the evaluation results are often inconsistent with the subjective feeling of the human being.

2) Structural similarity (SSIM). SSIM represents the criterion of similarity between image structures, which involves more categories than PSNR, such as contrast, brightness, and structure. As shown in (25), (26), (27):

$$l(I^0, I^1) = \frac{2u_{I^0}u_{I^1} + C_1}{u_{I^0}^2 + u_{I^1}^2 + C_1} \tag{25}$$

$$c(I^0, I^1) = \frac{2\sigma_{I^0}\sigma_{I^1} + C_2}{\sigma_{I^0}^2 + \sigma_{I^1}^2 + C_2} \tag{26}$$

$$s(I^0, I^1) = \frac{\sigma_{I^0 I^1} + C_3}{\sigma_{I^0}\sigma_{I^1} + C_3} \tag{27}$$

where u_{fo}, u_{f1} represents the mean of the corresponding image I^0, I^1, $\sigma_{f^0}, \sigma_{f^1}$ represents the image variance, $\sigma_{1^0 1^1}$ is the covariance between I^0 and I^1, and C_1, C_2 and C_3 are constants. The SSM results in a value range of [0, 1], which is inversely proportional to the degree of distortion of the image.

3) Perceptual Index (PI). The PI is an objective criterion that is used to measure the subjective evaluation of an image and is often found in image experiments framed by generative adversarial networks, as shown in Equation (28):

$$PI(I_s) = \frac{1}{2}((10 - Ma(I_s)) + NIQE(I_s)) \tag{28}$$

where I_s is the reconstructed image, $Ma(\cdot)$ represents the quality metric index of the reference-free image, and $NIQE(\cdot)$ is the metric index of the reference-free image evaluation. The perceptual index is closely related to the visual quality of the image, and is inversely related to the level of visual presentation of the image, the lower its value, the higher the perceptual quality of the image.

4. Analysis of the results of the optimization of the digital conservation and three-dimensional reconstruction of wall paintings

4.1. *Protection effects and analysis*

In order to verify the effectiveness of this paper's algorithm in mural image restoration, this paper takes the mural paintings of Yongle Palace in Shanxi as the experimental object, and evaluates and analyzes the algorithm's efficiency and restoration effect from two aspects. Considering that mural restoration is a pathological inverse problem, the actual broken mural paintings lack of intact comparison samples, so it is not possible to measure the degree of similarity by peak signal-to-noise ratio and structural similarity. In this case, in this paper, in order to further verify the performance of the proposed algorithm in this chapter, the algorithm is applied to the restoration experiments by adding artificial breakage to the intact preserved fresco images and then applying the algorithm to the restoration experiments. The peak signal-to-noise ratio (SNR) and the repair time are usually used to quantitatively compare the restoration effect of the cracked frescoes with artificial damages. The peak signal-to-noise ratio is statistically analyzed based on the gray value of the image pixels, and the larger the value is, the higher the image similarity is, i.e., the better the restoration effect is.

4.1.1. Experiments and analysis of restoration of artificially damaged murals. The following is a quantitative and objective analysis of the repair effect of the three algorithms in the repair experiment of the damaged mural painting of "Taishangjin". Figure 3 shows the relationship between different iterations and PSNR, repair time, Figure (a) is the PSNR value Figure (b) is the repair time.

Figure (a) represents the changes in the corresponding PSNR values of the three algorithms with the increase in the number of iterations for their repair images. It can be found that with the increase in the number of iterations in the early stage, the PSNR value of the restored image and its obvious positive correlation trend, this paper's algorithm in the number of iterations of 500 times, the PSNR is 39.755db. Iteration number and the PSNR value of the relationship between the later changes in the magnitude of the relationship is no longer so obvious, and gradually tends to stabilize.

Figure (b) represents the change of the corresponding repair time of various algorithms with the increase of the number of iterations. It can be found that when the number of iterations is the same, the repair process of the TV model takes the shortest time, and it takes 47.531s to complete the repair first. The traditional CDD model has the lowest repair efficiency because it needs to calculate the third-order partial differential for each point during the iteration process. On the contrary, the algorithm in this paper, due to the introduction of adaptive parameters, so that the model can choose different diffusion methods according to the curvature information, its repair efficiency is between the CDD algorithm and the TV algorithm, and the repair time is 54.816s.

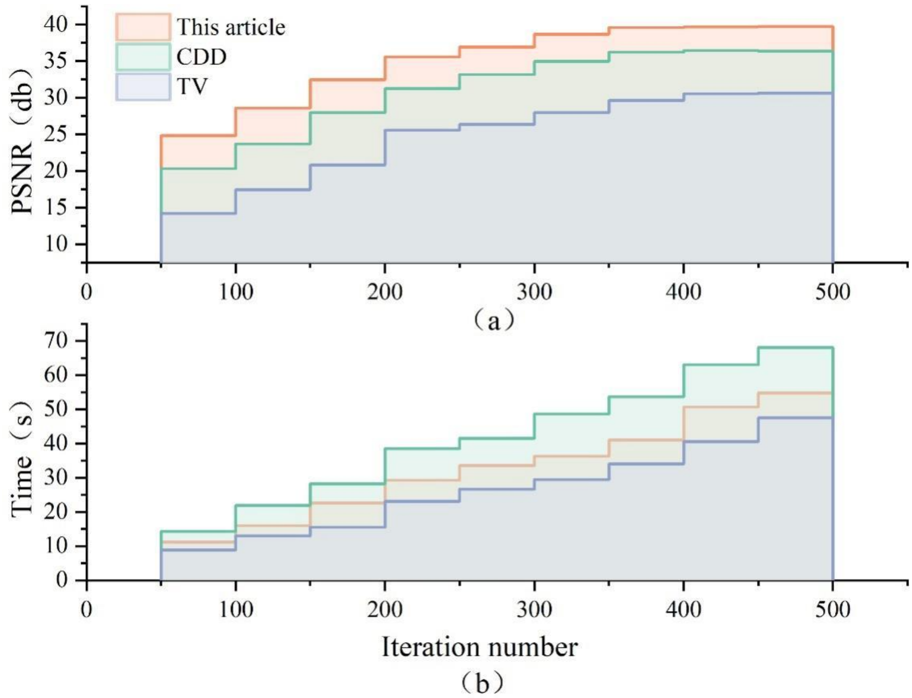

Fig. 3. The relationship between different iterations and PSNR as and repair time

It shows the comparison of PSNR and repair time of different algorithms for repair, and the table shows the comparison data of peak signal-to-noise ratio and repair efficiency of eight mural image samples repaired using three repair algorithms in the cracked mural repair experiment. It can be seen that this paper's algorithm can effectively repair the cracked region in the mural image while compromising the repair speed of the CDD model and the TV model, and has achieved better repair results in terms of repair efficiency and visual connectivity, which can effectively improve the problem of low repair efficiency and poor quality of repair of traditional curvature-driven models, so this paper's algorithm model is better than the other models in terms of comprehensive performance. When repairing artificially added broken murals, when the iterative repair tends to stabilize, this paper's algorithm improves the repair time by 9.545~15.625 seconds and the peak signal-to-noise ratio index by 1.35~4.769db compared with the traditional CDD algorithm.

Table 1. Comparison of PSNR and ssim values repaired by different algorithms

Image sample	TV model		CDD model		This algorithm	
	Repair time/s	PSNR	Repair time/s	PSNR	Repair time/s	PSNR
Sample 1	38.454	30.894	59.481	34.456	43.856	38.486
Sample 2	39.756	29.345	58.865	35.485	45.489	39.475
Sample 3	43.445	29.415	64.498	32.893	52.455	35.452
Sample 4	32.469	34.425	55.652	36.162	43.462	38.452
Sample 5	35.985	27.985	56.456	34.965	42.658	37.152
Sample 6	41.845	29.485	60.856	35.186	50.865	39.955
Sample 7	42.756	34.156	63.845	36.495	54.152	37.845
Sample 8	36.898	31.985	58.499	35.462	48.954	38.848

4.1.2. Subjective evaluation of the results of real mural restoration. In order to ensure the objectivity of the subjective review, the same assessment method as the previous ones was used, and 45 mural practitioners were randomly invited by the MOS method to assess the quality of the mural reconstruction and mural artistry, and the assessment criteria were divided into two aspects: global reconstruction quality, and detail reconstruction artistry. The global reconstruction quality was assessed from the reconstructed image color, contrast, and brightness, and the detailed reconstruction artistry was assessed from the detailed texture and artistry value. According to the above two aspects, the MOS scoring interval was set at [0,5], and the average value was calculated as the final MOS score after the statistical scoring results were made respectively. Table 2 shows the subjective score of mural reconstruction, according to the scoring results, the reconstructed mural images of this paper's algorithm are more in line with human subjective vision, and there are more obvious improvements in color, contrast, brightness, and the mean values of global reconstruction quality and detail reconstruction artistry are 4.09 and 4.191, respectively. in the evaluation of mural artistry, the mural industry personnel for the mural details of the texture, and the reconstructed images of the artistic value, all of which are give higher evaluation scores to this paper's method, which is better than the reconstructed images of other methods, and agree that the reconstructed images of this paper's algorithm are more artistic in terms of texture details.

Table 2. The mural reconstruction subjective score

Personnel	Algorithm					
	TV		CDD		This algorithm	
	1	2	1	2	1	2
1	3.275	2.329	3.233	5.253	3.770	4.646
2	1.815	1.470	3.752	5.532	2.839	4.057
3	4.188	0.898	3.893	3.569	2.564	3.614
4	3.811	2.721	3.388	4.214	4.182	4.559
5	3.870	2.294	3.075	2.911	5.536	3.747
6	4.384	2.231	4.443	2.494	2.229	3.554
7	1.960	3.178	5.085	2.910	2.729	4.331
8	4.795	1.993	2.870	2.319	3.966	5.730
9	3.758	2.329	4.365	2.877	1.502	4.385
10	2.239	3.832	3.832	4.105	3.864	3.676
11	4.086	1.344	5.193	4.613	4.729	5.174
12	3.024	3.679	4.933	3.067	2.939	3.662
13	2.492	1.675	5.029	4.425	4.200	4.797
14	3.381	1.648	3.400	3.508	6.668	4.595
15	3.295	3.488	5.259	4.565	4.616	5.180
16	3.938	0.833	2.687	3.504	1.289	3.623
17	2.133	4.990	2.267	3.808	3.514	2.591
18	3.050	3.968	5.295	4.529	3.255	6.736
19	4.789	3.564	4.978	5.182	6.158	3.631
20	2.784	3.129	3.442	4.822	3.154	5.443
21	4.475	4.947	2.652	4.076	5.673	4.707
22	3.010	3.123	2.647	4.929	5.061	2.995
23	4.255	3.732	4.269	3.849	4.002	2.198
24	2.904	4.704	4.465	4.901	6.119	4.704
25	3.147	3.512	3.793	3.530	6.572	4.834
26	3.002	4.125	2.759	4.063	4.522	3.460
27	1.856	4.736	1.401	3.886	4.485	2.878
28	2.441	3.905	3.365	4.507	4.957	3.975
29	1.632	2.622	3.292	4.681	4.242	3.574
30	5.642	2.983	5.325	3.220	3.851	6.350
31	2.890	2.321	3.384	3.212	1.922	2.909
32	2.302	0.132	3.631	5.639	4.797	3.233
33	3.576	4.502	1.963	2.489	4.672	4.700
34	3.755	3.267	5.105	2.251	5.287	4.308
35	3.377	3.006	3.767	1.778	4.930	6.274
36	2.603	3.225	2.465	2.809	5.230	3.321
37	4.844	4.054	3.623	4.182	5.056	4.674
38	4.250	4.136	5.046	5.255	4.055	4.459
39	3.220	2.021	3.717	3.160	3.566	4.969
40	3.685	4.202	5.589	3.611	5.524	1.845
41	2.583	2.875	4.170	3.267	3.308	4.272
42	3.695	1.936	5.173	3.704	3.779	3.655
43	1.231	4.036	4.150	0.790	1.083	4.081
44	4.699	4.830	5.080	5.080	3.577	4.507
45	2.034	4.255	4.863	4.869	4.088	3.971

4.1.3. Image Extraction Processing Effect. Figure 4 shows the comparison between target curvature and discrete curvature. The results of discrete curvature of straight line segments have a high degree of agreement with the target curvature calculation results, and the calculation results of circular arc segments have a relatively low degree of agreement, and the calculated values of discrete curvature of AB, CD and EF segments are in the range of -0.00945 to -0.00478, with an average value of -0.007115, which differs from the target curvature standard value by 6.477%, while the calculated values of FG segment discrete curvature The calculated value is in the range of 0.00596~-0.00865, and the average value is 0.007305, which is 6.715% different from the target curvature standard value. After the curvature is controlled within a certain range, the contour line is segmented, and the AB, CD, EF and FG segments are approximated as circular arcs, and the rest are approximated as straight line segments, and the calculation of the discrete curvature can satisfy the requirements of calculation accuracy. From the figure, it can be seen that the method can get the approximate target curvature, produce less redundant feature points, and have a strong adaptive ability.

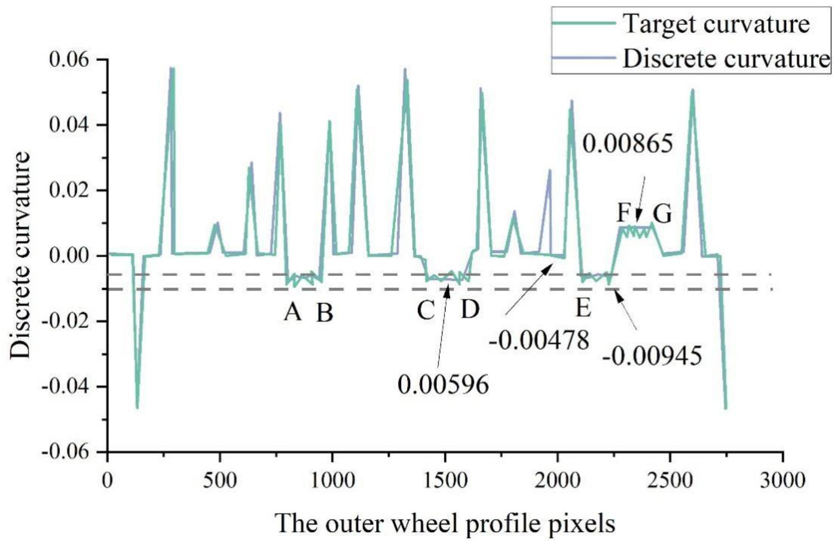

Fig. 4. The target curvature is compared to the discrete curvature

Figure 5 shows the results of the discrete curvature calculation. The curvature value threshold is determined by determining the curvature significant changes, so as to fit the segments. In the figure, the curvature of the AF segment is 0 and the boundary is fitted as a straight line, the curvature of the BC and DE segments is between -0.003512 and 0.003482, which can be approximated to be fitted as a straight line, the CD segments are fitted as arcs, and the rest of the segments are fitted as straight lines and arcs. By calculating the discrete curvature and determining the segmentation threshold of the outer contour graphic of the mural digitized image optimization results, the outer contour of the mural can be fitted by segments to provide an accurate data base for engineering design.

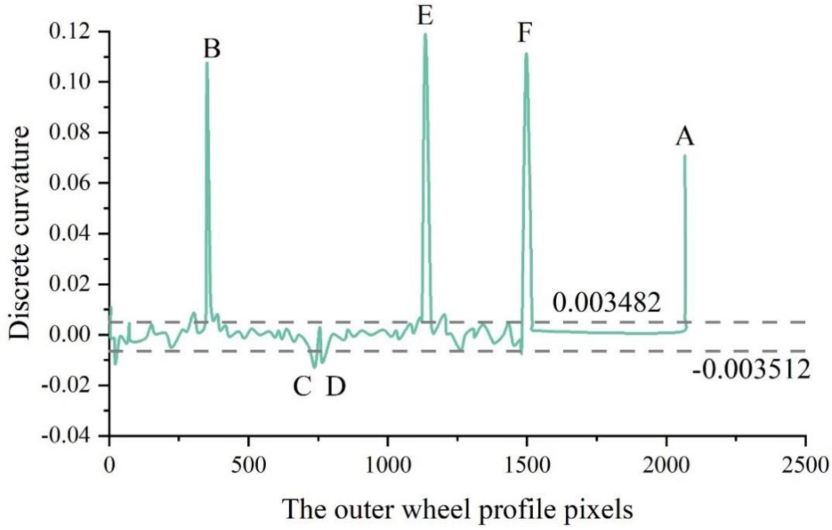

Fig. 5. The results of the discrete curvature calculation

4.2. Quality of digitized image reconstruction of wall paintings

Table 3 shows the comparison of reconstruction quality parameter values for the three types of mural images tested by different algorithms, demonstrating the results of PSNR and SSIM for 12 color mural images processed for super-resolution reconstruction using the different methods mentioned above and the method of this paper under the same experimental conditions. It can be seen from Table 3: for the restoration results of 12 color mural images, the two parameters of the method in this chapter - PSNR and SSIM - are higher than those of several other compared algorithms. In order to highlight the enhancement effect, the detailed comparison values of this paper's algorithm with other algorithms under different categories of mural images will be given below. In algal well category images, the mean value of PSNR index of this paper's method is improved by 1.462dB than that of MCcSR method, and the mean value of SSIM index is improved by 0.076, and in portrait and scene images, it has been improved to a different degree than other algorithms, so it can be seen that the method of this chapter is more effective in utilizing inter-channel correlation and retaining the inter-channel edge information of the color fresco images.

Table 3. Comparison of the reconstructed quality parameters of the mural image

Mural image		Parameter	BI	SCSR	QSCSR	MCcR	This method
Caisson chart	Test chart(a)	PSNR	21.897	23.585	23.785	25.865	25.945
		SSIM	0.752	0.753	0.756	0.769	0.856
	Test chart(b)	PSNR	27.595	27.459	32.287	30.254	33.468
		SSIM	0.915	0.925	0.945	0.945	0.954
	Test chart(c)	PSNR	23.748	24.896	29.756	28.456	29.915
		SSIM	0.715	0.816	0.816	0.816	0.915
	Test chart(d)	PSNR	23.756	24.863	25.863	26.456	27.552
		SSIM	0.612	0.816	0.713	0.746	0.856
	Mean value	PSNR	24.249	25.201	27.923	**27.758**	**29.220**
		SSIM	0.749	0.828	0.808	**0.819**	**0.895**
Portraits	Test chart(e)	PSNR	33.845	32.645	34.455	35.785	36.453
		SSIM	0.915	0.915	0.915	0.915	0.951
	Test chart(f)	PSNR	24.568	23.755	26.448	26.452	26.795
		SSIM	0.795	0.856	0.815	0.816	0.875
	Test chart(g)	PSNR	25.865	26.485	30.486	29.456	31.462
		SSIM	0.819	0.812	0.826	0.816	0.915
	Test chart(h)	PSNR	26.486	27.485	29.468	29.486	31.485
		SSIM	0.815	0.786	0.948	0.816	0.945
	Mean value	PSNR	27.691	27.593	30.214	30.295	31.549
		SSIM	0.836	0.842	0.876	0.841	0.922
Scene map	Test chart(i)	PSNR	29.456	30.856	31.486	32.384	33.489
		SSIM	0.858	0.815	0.918	0.914	0.934
	Test chart(j)	PSNR	25.426	27.562	28.754	28.462	30.915
		SSIM	0.756	0.865	0.815	0.816	0.945
	Test chart(k)	PSNR	26.463	28.486	30.865	29.445	32.562
		SSIM	0.852	0.815	0.915	0.904	0.954
	Test chart(l)	PSNR	27.466	28.875	30.489	31.878	31.975
		SSIM	0.846	0.868	0.915	0.945	0.955
	Mean value	PSNR	27.203	28.945	30.399	30.542	32.235
		SSIM	0.828	0.841	0.891	0.895	0.947

5. Conclusion

In this paper, we use digital image processing technology to denoise the fresco image, and adopt the improved wavelet transform to decompose and filter the high-frequency component and low-frequency component, and decompose the grayscale of the fresco image, and repair it respectively. Filtering, enhancement, detection and localization are carried out sequentially to complete the mural image edge detection. Combining the generative adversarial network and self-attention mechanism, the super-resolution 3D reconstruction of the fresco is realized. The PSNR value of the restored image of this paper's algorithm shows an obvious positive correlation trend, and when the number of iterations is 500 times, the PSNR reaches 39.755db, and the time for completing the restoration is 54.816s, which is at a medium level. In the subjective evaluation, the mean values of global reconstruction quality and detail reconstruction artistry of the frescoes restored and protected using the algorithms in this paper are 4.09 and 4.191, respectively, which are more artistic in texture detail processing. Comparing the target curvature and discrete curvature of the mural images processed through digitization, the calculated values of the discrete curvature of the AB, CD, and EF segments result in the range of -0.00945~-0.00478, and the mean value is -0.007115. The mean value of the PSNR index of the reconstruction method used in this paper improves by 1.462dB with the MCcSR method, and the mean value of the SSIM index improves by 0.076, which are improved to different degrees in different scenarios, and are more effective for digitized 3D reconstruction of murals.

References

[1] Yang, J., Cao, J., Yang, H., Li, Y., & Wang, J. (2021). Digitally assisted preservation and restoration of a fragmented mural in a Tang Tomb. Sensing and Imaging, 22, 1-18.

[2] Priego, E., Herráez, J., Denia, J. L., & Navarro, P. (2022). Technical study for restoration of mural paintings through the transfer of a photographic image to the vault of a church. Journal of Cultural Heritage, 58, 112-121.

[3] Han, H., & Lu, D. (2004, October). Computer aided protection and restoration of Dunhuang mural. In 2004 IEEE International Conference on Systems, Man and Cybernetics (IEEE Cat. No. 04CH37583) (Vol. 7, pp. 6434-6438). IEEE.

[4] Ren, H., Sun, K., Zhao, F., & Zhu, X. (2024). Dunhuang murals image restoration method based on generative adversarial network. Heritage Science, 12(1), 39.

[5] Tortora, M., Sfarra, S., Chiarini, M., Daniele, V., Taglieri, G., & Cerichelli, G. (2016). Non-destructive and micro-invasive testing techniques for characterizing materials, structures and restoration problems in mural paintings. Applied Surface Science, 387, 971-985.

[6] Wang, H. L., Han, P. H., Chen, Y. M., Chen, K. W., Lin, X., Lee, M. S., & Hung, Y. P. (2018). Dunhuang mural restoration using deep learning. In SIGGRAPH Asia 2018 technical briefs (pp. 1-4).

[7] Lv, C., Li, Z., Shen, Y., Li, J., & Zheng, J. (2022). SeparaFill: Two generators connected mural image restoration based on generative adversarial network with skip connect. Heritage Science, 10(1), 135.

[8] Shi, W., & Meng, X. P. (2024, June). Mural Restoration Research Based on Samples and Deep Learning. In 2024 IEEE International Conference on Information Technology, Electronics and Intelligent Communication Systems (ICITEICS) (pp. 1-4). IEEE.

[9] Cao, N., Lyu, S., Hou, M., Wang, W., Gao, Z., Shaker, A., & Dong, Y. (2021). Restoration method of sootiness mural images based on dark channel prior and Retinex by bilateral filter. Heritage Science, 9, 1-19.

[10] Wei, B., Liu, Y., & Pan, Y. (2003). Using hybrid knowledge engineering and image processing in color virtual restoration of ancient murals. IEEE Transactions on Knowledge and Data Engineering, 15(5), 1338-1343.

[11] Wang, Q., Hou, M., & Lyu, S. (2021). Virtual Restoration of Missing Paint Loss of Mural Based on Generative Adversarial Network. The International Archives of the Photogrammetry, Remote Sensing and Spatial Information Sciences, 46, 807-811.

[12] Zaitseva, V. (2022). Experience of restoration of murals of the Trinity gate church in Kyiv: Overview. International Journal of Conservation Science, 13(1), 85-94.

[13] Chanda, B., Ratra, D., & Mounica, B. L. S. (2012, November). Virtual restoration of old mural paintings using patch matching technique. In 2012 Third International Conference on Emerging Applications of Information Technology (pp. 299-302). IEEE.

[14] Li, H. (2021). Restoration method of ancient mural image defect information based on neighborhood filtering. Journal of Computational Methods in Sciences and Engineering, 21(3), 747-762.

[15] Cao, J., Zhang, Z., Zhao, A., Cui, H., & Zhang, Q. (2020). Ancient mural restoration based on a modified generative adversarial network. Heritage Science, 8, 1-14.

[16] Yan, Y., Gouet-Zhang, R., He, H., Lei, T., Zhang, X., & Jiang, C. (2024). Image Restoration Technology of Tang Dynasty Tomb Murals Using Adversarial Edge Learning. ACM Journal on Computing and Cultural Heritage.

[17] Li, J., Wang, H., Deng, Z., Pan, M., & Chen, H. (2021). Restoration of non-structural damaged murals in Shenzhen Bao'an based on a generator–discriminator network. Heritage Science, 9, 1-14.

[18] Xu, Z., Zhang, X., Chen, W., Liu, J., Xu, T., & Wang, Z. (2024). MuralDiff: Diffusion for Ancient Murals Restoration on Large-Scale Pre-Training. IEEE Transactions on Emerging Topics in Computational Intelligence.

[19] Kumar, K. M. P., Kumar, M., Bhargav, B. V. S., & Ghorai, M. (2014, January). Digital restoration of deteriorated mural images. In 2014 Fifth International Conference on Signal and Image Processing (pp. 36-41). IEEE.

[20] Cao, J., Li, Y., Zhang, Q., & Cui, H. (2019). Restoration of an ancient temple mural by a local search algorithm of an adaptive sample block. Heritage Science, 7(1), 39.

[21] Liu, Z. (2021, August). Yunnan ancient mural restoration based on deep learning. In Journal of Physics: Conference Series (Vol. 1992, No. 2, p. 022106). IOP Publishing.

[22] Xu, W., & Fu, Y. (2023). Deep learning algorithm in ancient relics image colour restoration technology. Multimedia Tools and Applications, 82(15), 23119-23150.

[23] Gao, Z., Du, M., Cao, N., Hou, M., Wang, W., & Lyu, S. (2023). Application of hyperspectral imaging technology to digitally protect murals in the Qutan temple. Heritage Science, 11(1), 8.

[24] Purkait, P., & Chanda, B. (2012, December). Digital restoration of damaged mural images. In Proceedings of the Eighth Indian Conference on Computer Vision, Graphics and Image Processing (pp. 1-8).

[25] Ahmad A. Alzahrani. (2024). Enhanced multimodal medical image fusion via modified DWT with arithmetic optimization algorithm. Scientific Reports(1),19261-19261.

[26] Dongyang Fu,Shangfeng Du,Yang Si,Yafeng Zhong & Yongze Li. (2024). Dynamic Tracking Matched Filter with Adaptive Feedback Recurrent Neural Network for Accurate and Stable Ship Extraction in UAV Remote Sensing Images. Remote Sensing(12),2203-2203.

[27] Jingyu Wang,Cheng Chen,Feiping Nie & Xuelong Li. (2024). Discriminative and robust least squares regression for semi-supervised image classification. Neurocomputing127316-.

[28] Xinjia Li,Yang Liu,Mingze Sun,Zhan Yu,Yue Li,Dan Zhao... & Xin Zhou. (2024). Computational ghost image encryption method based on sparse speckles. Physica Scripta(2),

[29] XiaoPing Ji,Shiyu Zhu,Yunlong Sun,Hangle Li,Ye Chen & Yun Chen. (2024). Reconstruction and evolution of 3D model on asphalt pavement surface texture using digital image processing technology and accelerated pavement testing. Road Materials and Pavement Design(8),1694-1719.